Nano Energy 32 (2017) 433–440

Contents lists available at ScienceDirect

Nano Energy

journal homepage: www.elsevier.com/locate/nanoen

Full paper

Impacts of surface or interface chemistry of ZnSe passivation layer on the performance of CdS/CdSe quantum dot sensitized solar cells

Fei Huang[a,b], Juan Hou[c], Hongen Wang[a], Hao Tang[a], Zhaoyu Liu[a], Lisha Zhang[b], Qifeng Zhang[a], Shanglong Peng[a], Jianshe Liu[b,*], Guozhong Cao[a,*]

[a] Department of Materials Science and Engineering, University of Washington, Seattle, WA 98195-2120, United States
[b] College of Environmental Science and Engineering, Donghua University, Shanghai 201620, PR China
[c] Key Laboratory of Ecophysics and Department of Physics, School of Science, Shihezi University, Xinjiang 832003, PR China

ARTICLE INFO

Keywords:
Quantum dot sensitized solar cell
ZnSe passivation layer
SILAR immersion sequence
Surface or interface chemistry
Charge recombination

ABSTRACT

ZnSe deposited via successive ionic layer adsorption and reaction (SILAR) method onto TiO_2/CdS/CdSe photoanode has been proven as an effective passivation layer to suppressing charge recombination and enhancing power conversion efficiency in quantum dot-sensitized solar cells (QDSCs). However, the device performance varies appreciably with the deposition process as the chemical identity and the interfacial structure between the passivation layer and the quantum dots and electrolytes have retained quite some unanswered questions. The present paper reports the significant impacts of ZnSe passivation layer with different surface or interface chemistry on the performance of CdS/CdSe QDSCs. The photovoltaic properties show that the performance of assembled cells has a strong dependence on the SILAR immersion sequences started with Zn^{2+} or Se^{2-}. When Zn^{2+} was initially deposited, the unintentionally formed QDs/ZnSe/Se/SeO_2 structure with a large amount of ZnSe leads to a significant increase in the photovoltaic properties. When Se^{2-} was first deposited, most of the Se^{2-} absorbed on the surface of the photoanode would be oxidized to form Se^0 and SeO_2, with a small fraction of ZnSe formed. The resulted QDs/Se/SeO_2/ZnSe structure leads to a drastic decrease of the solar cell performance.

1. Introduction

Excitonic solar cells have gained much attention, due to low materials cost, simple solution fabrication process with low energy consumption, and relatively high solar energy to electricity conversion efficiency [1–3]. Among various excitonic solar cells, dye sensitized solar cells (DSCs) have attracted intensive study for over 25 years since 1991 [4–6]. Quantum dot sensitized solar cells (QDSCs) have emerged as another low-cost solar cells due to their unique advantages derived directly from quantum dots, such as tunable band gap, high absorption coefficient, large dipole moment, and solution processability [7–10]. In addition, the theoretical power conversion efficiency of QDSCs can be reached as high as 44%, which surpassed the Shockley–Queisser limit in view of the hot electron extraction and multiple exciton generation (MEG) effect [11–13]. In recent years, the development of QDSCs has achieved great progress with their power conversion efficiency (PCE) increased continuously up to 11%, which is close to 13% for DSCs under one full sun illumination [14,15].

Two important factors that influence the photovoltaic properties of QDSCs are the capability of light absorption and charge separation and collection. Several approaches have been attempted to enhance light absorption, for example, introducing plasmonic metal nanoparticles (e.g. Au and Ag NPs) [16–18] and applying hierarchically structured electrodes with a scattering layer in QDSCs [19,20]. In addition to the enhancement of light absorption, more efforts have been put forward to reduce surface charge recombination, which is the main challenge limiting the charge collection capability, including interfacial charge recombination between QDs and electrolyte due to imperfect QDs surface, interfacial charge recombination between TiO_2 (when TiO_2 is used to form mesoporous photoanode) and electrolyte due to direct exposure of bare TiO_2 surface in the electrolyte [21–23]. The most commonly used method to reduce charge recombination is passivation treatment of the oxide photoanode and QDs, and significant improvement in PCE has been achieved through charge recombination control [24,25]. For example, a thin TiO_2 nanoparticle layer on the surface of ZnO mesoporous photoelectrode was found to decrease the surface charge recombination [26]. A novel double barrier coating treatment, by sequentially depositing optimized ZnS and SiO_2 layer on the

* Corresponding authors.
E-mail addresses: jiansheliu@dhu.edu.cn (J. Liu), gzcao@u.washington.edu (G. Cao).

http://dx.doi.org/10.1016/j.nanoen.2016.12.047
Received 16 November 2016; Received in revised form 23 December 2016; Accepted 24 December 2016
Available online 26 December 2016

quantum dot sensitized photoanode, was reported to increase the PCE from 6.37% to 8.37% [27] in comparison with single ZnS coating.

Various types of QDs have been adopted in QDSCs, such as CdS, [28] CdSe, [29,30] PbS, [22,31] PbSe, [32] Ag_2S, [33] $CuInS_2$ [34] and their hybrid structures, which can absorb light in the visible and near IR-regions. There are several methods to depositing QDs on the surface of wide band gap metal oxide semiconductors, such as TiO_2, ZnO and SnO_2, mainly through either self-assembled monolayer, deposition of pre-synthesized QDs by linker (bifunctional surface modifiers) assisted adsorption [35,36] or in-situ deposition of QDs by chemical bath deposition (CBD) and successive ionic layer adsorption and reaction (SILAR) [37,38]. For the first method, it is easy to control the shape, size and size distribution of the QDs with high crystallinity, and the obtained QDs can form compact and uniform coverage on the photoanode. Based on this method, a series of high efficiency records have been obtained [39–41]. As for the second method, the QDs' intimate connection with the oxide (TiO_2 or ZnO) photoanode leads to efficient charge transport, and the surface coverage can be easily controlled with low fabrication cost. While, the low temperature processing condition leads to an imperfect QDs surface with defects, permitting serious interfacial charge recombination. CdS/CdSe quantum dots co-sensitized solar cells fabricated via CBD or SILAR deposition method have been intensively investigated [42,43]. Interface charge recombination can be at least partially circumvented through the introduction of passivation layer; for example, ZnSe and ZnS with appropriate coverage and thickness could act as an efficient passivation layer in TiO_2/CdS/CdSe QDSCs [38,44]. In comparison with the most commonly used ZnS passivation layer, an enhancement in power conversion efficiency was obtained from 4.9% to 6.4% when ZnSe was used as a passivation layer [45]. However, the performance of the solar cells was found to exhibit a strong dependence on the SILAR deposition sequence. In this work, a systematic investigation has been carried out to understand the impacts of the chemical composition and interfacial structure of ZnSe passivation layer prepared via different SILAR sequences with Zn^{2+} initially deposited or otherwise Se^{2-} initially deposited. This will help to shed some light on how the different chemical composition and interfacial structure of ZnSe passivation layer could influence the performance of QDSCs. With Zn^{2+} initially deposited, a ZnSe/Se°/SeO_2 layer with a large amount of ZnSe was formed and acted as a passivation layer to hinder the overall charge recombination; with Se^{2-} initially deposited, a Se°/SeO_2/ZnSe layer with large amount of Se°/SeO_2 and a small amount of ZnSe was formed, which hinders the charge transport and serve as recombination center to decrease the photovoltaic properties. Se° was observed in both structures and contributed to a much enhanced light adsorption.

2. Results and discussion

Fig. 1(a) is the schematic illustration of the SILAR process for ZnSe passivation layer deposition. There are two precursor solutions for

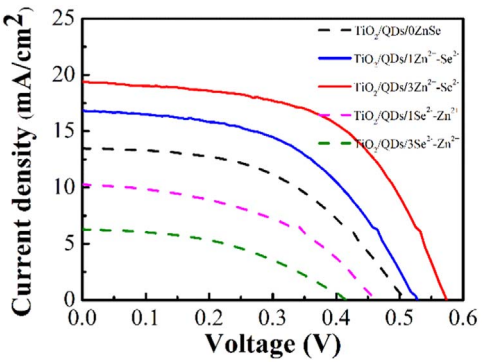

Fig. 2. I-V curves of the TiO_2/CdS/CdSe QDSCs deposited with various cycles of SILAR in Zn^{2+}-initiated and Se^{2-}-initiated sequences.

SILAR deposition ZnSe passivation layer. One is Zn^{2+} cationic solution, and another one is Se^{2-} anionic solution which filled with Argon during the deposition process to prevent selenium anions from oxidation in air. In the SILAR deposition process, the substrate QD sensitized photoanodes were dipped in each precursor solution for a certain period of time, followed with thorough rinsing and drying in air. Two types of ZnSe passivation layers were prepared on the surface of TiO_2/CdS/CdSe photoanodes via SILAR deposition with different immersion cycles and sequences, shown in Fig. 1(a), designated as Zn^{2+}-initiated sequence (1) Zn^{2+}-Se^{2-} and Se^{2-}-initiated sequence (2) Se^{2-}-Zn^{2+}. The SEM images in Fig. 1(b) show the surface characteristics of the TiO_2/CdS/CdSe photoanodes with 3 cycles of SILAR in Zn^{2+}-initiated and Se^{2-}-initiated sequences. The image of the TiO_2/QDs photoanode shows the mesoporous structure of the film. The images of TiO_2/QDs/3 Zn^{2+}-Se^{2-} and TiO_2/QDs/3 Se^{2-}- Zn^{2+} photoanodes show a subtle increase in TiO_2 particle size, comparing to the one without ZnSe passivation layer.

Fig. 2 shows the J-V curves of the solar cells with different ZnSe passivation layers formed with different SILAR deposition cycles and sequences, measured under the illumination of 100% sun (AM 1.5, 100 mW cm^{-2}). The corresponding photovoltaic properties, including the short-circuit current density (J_{sc}), the open circuit voltage (V_{oc}), the fill factor (FF) and the power conversion efficiency (Ƞ) obtained from the J-V curves are summarized and compared in Table 1. Apparently, there is a strong dependence between the photovoltaic performance and the SILAR immersion sequences for the deposition of ZnSe passivation layer. With the Zn^{2+}-initiated sequence, the values of J_{sc}, V_{oc} and FF all increased monotonically with the increasing SILAR deposition cycles. The cell exhibits a J_{sc} of 19.40 mA cm^{-2}, a V_{oc} of 0.57, and an FF of 0.56, yielding a maximum power conversion efficiency of 6.26% with three-cycle deposition. It should be noted that a further increase in SILAR cycles would result in a sharp reduction in all photovoltaic parameters due to the partial clogging of the mesoporous structure in the photoanode by the excessive ZnSe [45]. Whereas,

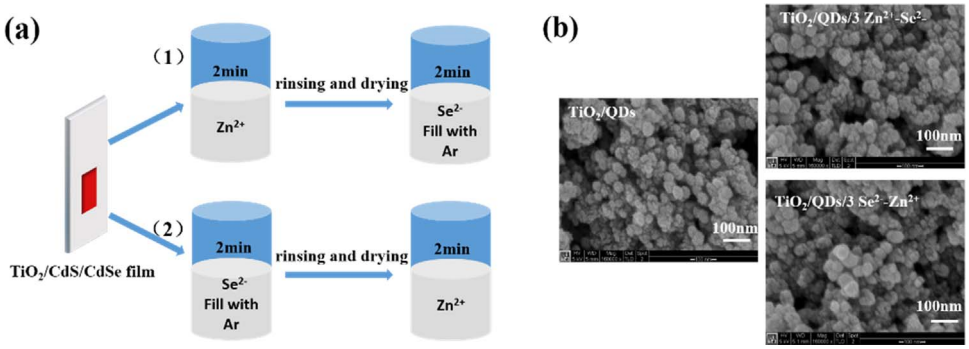

Fig. 1. (a) Schematic illustration of the typical SILAR procedures and (b) SEM images of TiO_2/QDs photoanodes and the photoanodes with 3 cycles of SILAR in Zn^{2+}-initiated and Se^{2-}-initiated sequence.

Table 1
Photovoltaic properties of the TiO_2/CdS/CdSe QDSCs deposited with various cycles of SILAR in Zn^{2+}-initiated and Se^{2-}-initiated sequences obtained from the J–V curves.

Samples	V_{oc} (V)	J_{sc} (mA cm^{-2})	FF	η (%)
TiO_2/QDs/0 ZnSe	0.51	13.51	0.50	3.39
TiO_2/QDs/1 Zn^{2+}-Se^{2-}	0.53	16.82	0.51	4.53
TiO_2/QDs/3 Zn^{2+}-Se^{2-}	0.57	19.40	0.56	6.26
TiO_2/QDs/1 Se^{2-}-Zn^{2+}	0.46	10.28	0.48	2.11
TiO_2/QDs/3 Se^{2-}-Zn^{2+}	0.41	6.27	0.44	1.15

with opposite SILAR immersion sequence, the photovoltaic performance parameters demonstrated opposite trend with all decreased with increased cycles of ZnSe deposition.

To determine the valence states of Se element and the chemical composition of the passivation layers deposited with different SILAR deposition sequences, X-ray photoelectron spectroscopy (XPS) analysis was performed. Fig. 3(a) and (b) displays the Se region of the high-resolution spectra for the TiO_2/CdS/CdSe films with three cycles of SILAR in Zn^{2+}-initiated and Se^{2-}-initiated sequences. The C1 peak position at 284.8 eV was used as reference to calibrate the spectrum. As indicated in these two spectra, the binding energy of Se 3d peaks can be fitted into eight peaks [46]. 3d 5/2 and 3d 3/2 peaks at 53.9 and 54.8 eV belong to CdSe; 3d 5/2 and 3d 3/2 peaks at 54.1 and 55.2 eV were assigned to ZnSe; 3d 5/2 and 3d 3/2 peaks at 55.1 and 55.6 eV were attributed to Se°; [46,47] and 3d 5/2 and 3d 3/2 peaks at the higher binding energy of 58.5 and 59.6 eV were for SeO_2 [46]. This result shows not only ZnSe existed on the surface, but Se° and SeO_2 was also formed as well via unavoidable oxidation. By integrating the surface area of the peaks, the intensity ratio of CdSe: ZnSe: Se°: SeO_2 are summarized in Table 2 [48]. For the passivation layer with 3 cycles of SILAR in Se^{2-}-initiated sequence, ZnSe only makes up to 5%, and most of the Se^{2-} were oxidized to Se° or SeO_2. While for the sample with three cycles of SILAR in Zn^{2+} initiated sequence, ZnSe takes up a large portion of 21.1%, while Se° and SeO_2 only account for 8.3% and 1.7%, respectively.

In the Zn^{2+}-initiated SILAR immersion sequence, precursor solutions of Zn^{2+}($Zn(Ac)_2$·$2H_2O$) and Se^{2-}(Se powders were reduced via sodium borohydride), both 100 mM in DI water were prepared. The formation of ZnSe took place via the following steps:

The reduction of Se to Se^{2-}: [49,50]

$$Se + BH^{4-} \rightarrow Se^{2-} + H_2 + 2BH_3 \quad (1)$$

The release of Zn^{2+} from $Zn(OAc)_2$ in the cationic precursor solution:

$$Zn(OAc)_2 \rightarrow Zn^{2-} + 2OAc^{-} \quad (2)$$

When the TiO_2/CdS/CdSe film was immersed in Zn^{2+} contained solution, Zn^{2+} ions were adsorbed onto the surface. After immersed the film in Se^{2-} ion contained solution, the following reaction takes place:

$$Zn^{2+} + Se^{2-} \rightarrow ZnSe \quad (3)$$

According to XPS results, Under current operational environment, the Se^{2-} ions on the surface of ZnSe layer would partially oxidized to Se° and SeO_2 in air during the rinsing and drying process, the oxidation of the Se^{2-}:

$$Se^{2-} + \frac{1}{2}O_2 \rightarrow Se^0 \quad (4)$$

$$Se^{2-} + O_2 \rightarrow SeO_2 \quad (5)$$

Thus, a TiO_2/QDs/ZnSe/Se°/SeO_2 structure was formed unintentionally.

While, in the Se^{2-}-initiated SILAR immersion sequence, when the TiO_2/CdS/CdSe film was immersed in Se^{2-} contained solution, Se^{2-} ions adsorbed onto the surface. Before immersed the film into the Zn^{2-} contained solution, the Se^{2-} on the surface of the film would be partially oxidized to Se° and SeO_2 before combine with Zn^{2+} to form ZnSe during the rinsing and drying process in air. When the film was immersed in Zn^{2+} contained solution, the remaining Se^{2-} combined with Zn^{2+} to form ZnSe. As a result, a TiO_2/QDs/Se°/SeO_2/ZnSe structure was formed.

To investigate the influence of the SILAR immersion sequences on the optical properties of the TiO_2/CdS/CdSe photoanodes, Fig. 4 illustrates the light absorption of TiO_2/CdS/CdSe photoanodes with different SILAR immersion sequences as well as different deposition cycles. Compared with the photoanode without ZnSe deposition, all the

Table 2
Binding energy of Se 3d levels after fitting process.

3 Zn^{2+}-Se^{2-}	XPS line	Peak ID	Band Energy	Group %	Assignment
	Se 3d5/2	PK 1	53.89	41.3	
	Se 3d3/2	PK 2	54.80	27.6	68.9% CdSe
	Se 3d5/2	PK 3	54.13	12.7	
	Se 3d3/2	PK 4	55.20	8.1	21.1% ZnSe
	Se 3d5/2	PK 5	55.09	5.0	
	Se 3d3/2	PK 6	55.60	3.3	8.3% Se
	Se 3d3/2	PK 7	58.90	1.0	
	Se 3d5/2	PK 8	59.80	0.7	1.7% SeO_2
3 Se^{2-}-Zn^{2+}	XPS line	Peak ID	Band Energy	Group %	Assignment
	Se 3d5/2	PK 1	53.83	50.5	
	Se 3d3/2	PK 2	54.76	33.5	84% CdSe
	Se 3d5/2	PK 3	54.19	3.1	
	Se 3d3/2	PK 4	55.20	2.1	5.2% ZnSe
	Se 3d5/2	PK 5	55.10	3.2	
	Se 3d3/2	PK 6	55.68	2.1	5.3% Se
	Se 3d3/2	PK 7	58.66	3.4	
	Se 3d5/2	PK 8	59.71	2.2	5.5% SeO_2

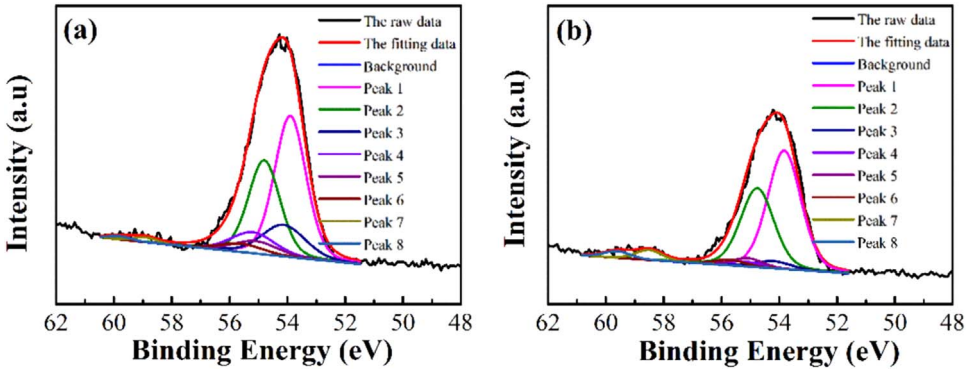

Fig. 3. X-ray photoelectron spectra of the Se 3d peaks for TiO_2/CdS/CdSe photoanodes deposited with three cycles of SILAR in (a) Zn^{2+}-initiated and (b) Se^{2-}-initiated sequences after fitting process.

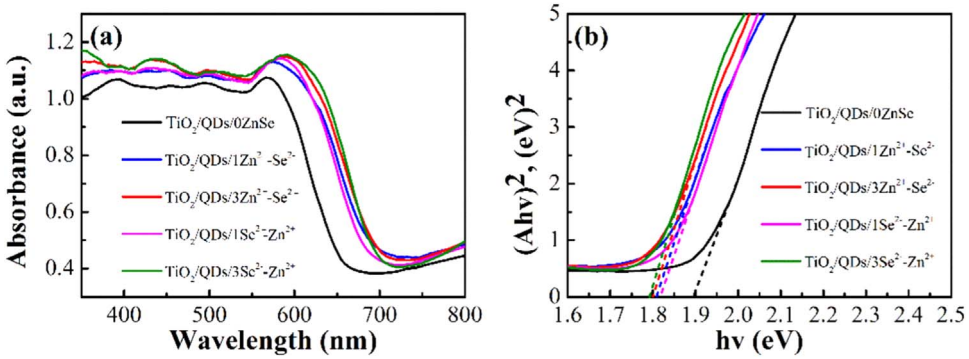

Fig. 4. (a) UV–visible light absorption spectra and (b) $(Ahv)^2$ vs. *hv* curves of TiO_2/CdS/CdSe films deposited with various cycles of SILAR in Zn^{2+}-initiated and Se^{2-}-initiated sequences.

other four photoanodes with a ZnSe passivation layer show a similar trend with enhanced light absorbance and a noticeable red-shift in absorption edge. Fig. 4(b) shows the band gap of the QDs estimated by extrapolating the linear portion of the $(Ahv)^2$ versus *hv* plots, according to Eq. (6), where A is the absorbance, c is a constant, υ is the frequency and h is Plank's constant [51,52].

$$(Ahv)^2 = c(hv - E_g) \quad (6)$$

The band gap of the CdSe and CdS QDs without the introduction of ZnSe passivation layer is calculated to be ~1.9 eV, much larger than the band gap of bulk CdSe (1.74 eV) and bulk CdS (2.4 eV) as a result of quantum confinement effect. With the introduction of ZnSe passivation layer using various cycles of SILAR in Zn^{2+}-initiated and Se^{2-}-initiated sequences, the nominal band gap reduces to ~1.8 eV, corresponding with the red shift of the absorption edge, though still appreciably larger than that of bulk CdSe and CdS.

Since ZnSe has a band gap, 2.7 eV, larger than that of CdS and CdSe quantum dots, the absorption of ZnSe would not result in a broader absorption range towards the longer wavelength region. The increased light absorption (intensity) and the red shift absorption edge might be attributed to two possible mechanisms. Firstly, as proposed and discussed in the literatures, [53,54] ZnSe passivation layer could form a type II core-shell structure with CdS/CdSe quantum dots as schematically shown in Scheme 1, due to the interaction of the two parts, excitons could be created by exciting the electrons from the valence band of ZnSe QDs to the conduction band of CdSe QDs, which would consequently result in an enhanced light absorption and extended the absorption edge to 886 nm. However, this mechanism would not be able to explain why the nominal bandgap is ~1.8 eV. Secondly, EDS results in Fig. 5 showed that there must be excessive Cd^{2+} existing on the surface of the TiO_2/CdS/CdSe films. When the ZnSe passivation layer was deposited first with Se^{2-} precursor solution, the excessive Cd^{2+} on the CdSe quantum dot surface will combine with Se^{2-} to form CdSe, leading to further growth of CdSe quantum dots. In

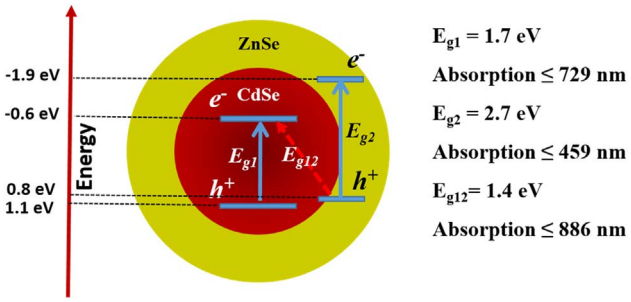

Scheme 1. Type-II band alignment in CdSe/ZnSe Core/Shell QDs. (Direct bandgap excitation: E_{g1} (ZnSe) ~2.7 eV, E_{g2} (CdSe) ~1.7 eV. Indirect bandgap excitation: E_{g12} (CdSe/ZnSe) ~1.4 eV. Band offset: Ub (conduction band) ~−0.6 eV, Uh (valence band) ~0.8 eV. All values correspond to bulk parameters [53,55,56]).

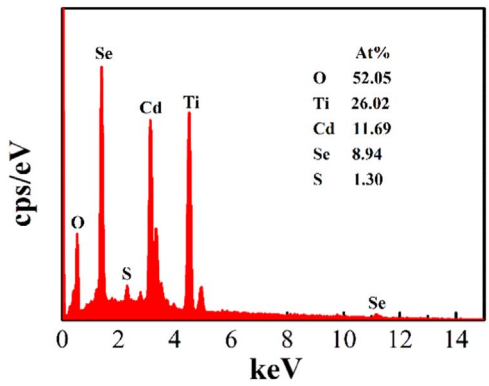

Fig. 5. Energy dispersive X-ray spectrum of the TiO_2/CdS/CdSe photoanode.

this case, light absorbance is expected to increase and the bandgap of the quantum dots would reduce with light absorption edge extended to longer wavelength. Although this hypothesis may explain the red shift of light absorption and increased light absorption intensity when the CdSe quantum dots loaded photoanodes were first immersed in Se^{2-} precursor solution for the deposition of ZnSe passivation layer; it could not explain the same enhancement of light absorbance and red shift in the samples when the ZnSe layer was deposited first with Zn^{2+} precursor solution.

Although these two assumptions may partially explain the improved light absorption, there is another factor that contributes to the enhancement according to the XPS results. XPS shows not only the existence of ZnSe on the surface of the photoanodes, but also the Se° and SeO_2 formed from the oxidation of the Se^{2-} when exposed to the air. It was reported that, as a narrow bandgap (1.8 eV) semiconductor, Se has been used as light absorber in solar cells. [57] Its light absorption can extend to 689 nm, which fits well with the red-shift of light absorption for the photoanodes deposited with ZnSe. In order to evaluate the influence of the Se° on light absorption of the SILAR deposited ZnSe, ZnSe layer was deposited on the surface of TiO_2 film with 5 cycles of SILAR in Zn^{2+}-initiated sequence. Fig. 6(a) shows the UV–vis absorption spectra of the TiO_2, TiO_2/ZnSe (Ar), TiO_2/ZnSe (air) films. The TiO_2/ZnSe (Ar) film was stored in Argon before the characterization. While, the TiO_2/ZnSe (air) was stored in air. A picture of TiO_2, TiO_2/ZnSe (Ar), TiO_2/ZnSe (air) films is shown as inset in Fig. 6(a). It can be clearly seen that the color of TiO_2/ZnSe (Ar) is light yellow with the absorption edge at 470 nm. After exposure to air for several minutes, the color of TiO_2/ZnSe (air) film changed to orange with the absorption edge at about 600 nm. The band gap of the TiO_2/ZnSe (Ar) film estimated according to Eq. (6) is about 2.65, as shown in Fig. 6(b), closing to the band gap of bulk ZnSe (2.7 eV). However, the absorption beyond 470 nm for the TiO_2/ZnSe (Air) sample could not be caused by ZnSe itself. It was possibly attributed to the presence of Se°

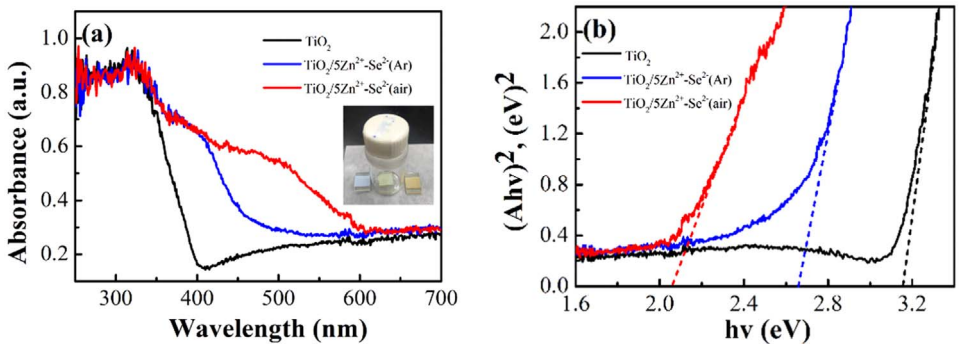

Fig. 6. (a) UV–visible light absorption spectra and (b) $(Ahv)^2$ vs. hv curves of the TiO_2 films and the TiO_2 films deposited with five cycles of SILAR in Zn^{2+}-initiated sequence. (The TiO_2/5 Zn^{2+}-Se^{2-} (Ar) film was stored in Argon before the characterization. While, the TiO_2/5 Zn^{2+}-Se^{2-} (air) film was stored in air.).

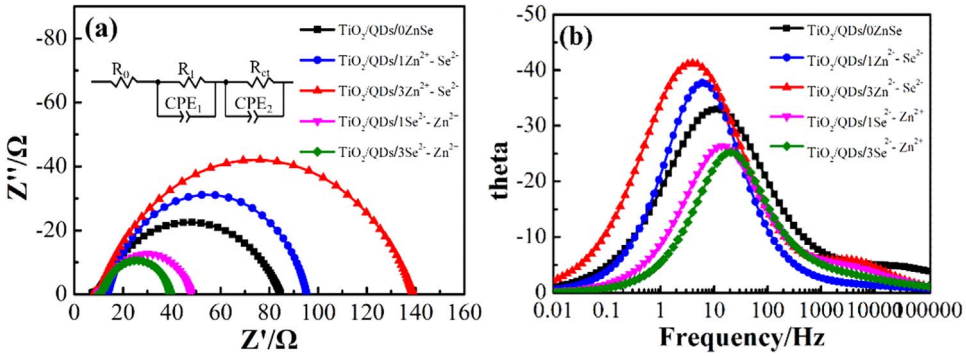

Fig. 7. (a) Nyquist plots and (b) Bode plots of EIS spectra of TiO_2/CdS/CdSe QDSCs deposited with various cycles of SILAR in Zn^{2+}-initiated and Se^{2-}-initiated sequences recorded under dark at an applied forward bias of −0.6 V.

with quantum confinement effect.

Electrochemical impedance spectra (EIS) of the solar cells were characterized. Fig. 7 presents the EIS results of the TiO_2/CdS/CdSe QDSCs deposited with ZnSe passivation layer using various SILAR cycles of Zn^{2+}-initiated and Se^{2-}-initiated sequences, which were fitted with Z-view software based on the equivalent circuit in the inset of Fig. 7(a). The fitting results of the electrochemical impedance spectra are shown in Table 3. The Nyquist plot contains two semicircles. The first small semicircle corresponds to R_1, which represents the charge transfer resistance at counter electrode/electrolyte interface. The second big semicircle corresponding to R_{ct}, represents the charge transfer resistance at TiO_2/QDs/electrolyte interfaces and within the TiO_2 films. There is a big difference between these samples in R_{ct}. The value of R_{ct} dramatically increased with more cycles of SILAR in Zn^{2+}-initiated sequence. When three cycles were applied, the value of R_{ct} reached 129.2 Ω, which is significantly higher than 74.7 Ω of the QDSCs without ZnSe passivation layer. Whereas, for Se^{2-}-initiated sequence, the value of R_{ct} decreased with more cycles of SILAR. Since R_{ct} represents the charge recombination resistance at TiO_2/QDs/electrolyte interfaces and within the TiO_2 films, a higher R_{ct} indicates the charge recombination at these interfaces is less likely to occur [58]. Fig. 7(b) shows the Bode plots of the TiO_2/CdS/CdSe QDSCs deposited with various cycles of SILAR in Zn^{2+}-initiated and Se^{2-}-initiated sequences. The curve peak of the spectrum can be used to determine the electron lifetime (τ_n) according to Eq. (7): [59]

$$\tau_n = \frac{1}{\omega_{min}} = \frac{1}{2\pi f_{min}} \quad (7)$$

where f_{min} is the peak frequency at the minimum phase angle in the bode plots. The corresponding electron lifetime of the QDSCs are listed in Table 3. The electron lifetime shows the same trend with the R_{ct}. Increase in both R_{ct} and τ_n implies a reduced interface charge recombination in QDSCs. This result reveal that, the ZnSe/Se/SeO_2 layer formed with Zn^{2+}-initiated sequence contains large amount of ZnSe and less Se/SeO_2 has superior ability to hinder the overall charge recombination. On the contrary, the Se/SeO_2/ZnSe layer formed with Se^{2-}-initiated sequence contains large amount of Se/SeO_2 and less ZnSe would lead to serious charge recombination.

Table 3
The fitting results of the Electrochemical impedance spectra.

Samples	R_1 (Ω)	R_{ct} (Ω)	τ_n (ms)
TiO_2/QDs/0 ZnSe	2.8	74.7	14.2
TiO_2/QDs/1 Zn^{2+}-Se^{2-}	2.1	81.2	26.4
TiO_2/QDs/3 Zn^{2+}-Se^{2-}	2.0	129.2	49.3
TiO_2/QDs/1 Se^{2-}-Zn^{2+}	2.6	35.4	11.5
TiO_2/QDs/3 Se^{2-}-Zn^{2+}	2.6	26.9	7.6

The separation and transfer of photo-excited electrons and holes across the interfacial region in the TiO_2/CdS/CdSe QDSCs with three cycles of SILAR in Zn^{2+} and Se^{2-}-initiated sequences are shown in Scheme 2 (a) and (b). According to the XPS analysis, for the solar cells with various cycles of SILAR in Zn^{2+}-initiated sequence, when immersing the TiO_2/QDs/Zn^{2+} photoanode into Se^{2-} solution, the Zn^{2+} will combine with Se^{2-} to form ZnSe first, then the excess Se^{2-} on the surface will be oxidized to Se^0/SeO_2 during the rinsing and drying process. A TiO_2/QDs/ZnSe/Se^0/SeO_2 structure was formed unintentionally as illustrated in Schematic 2 (a). While for the solar cells with various cycles of SILAR in Se^{2-}-initiated sequence, most of Se^{2-} would be oxidized to Se^0/SeO_2 during the rinsing and drying process before combining with Zn^{2+} to form ZnSe. In this case, a TiO_2/QDs/Se^0/SeO2/ZnSe structure formed as shown in Schematic 2 (b). In the solar cells, under light illumination, CdS/CdSe QDs absorb photons and generate electron-hole pairs, which will separate into electrons and holes instantly. The electrons will subsequently transfer to the conduction band of TiO_2 and holes will transfer to the electrolyte and then reduced by the redox couple. At the same time, charge recombination processes take place mainly at the interfaces of TiO_2/QDs/electrolyte

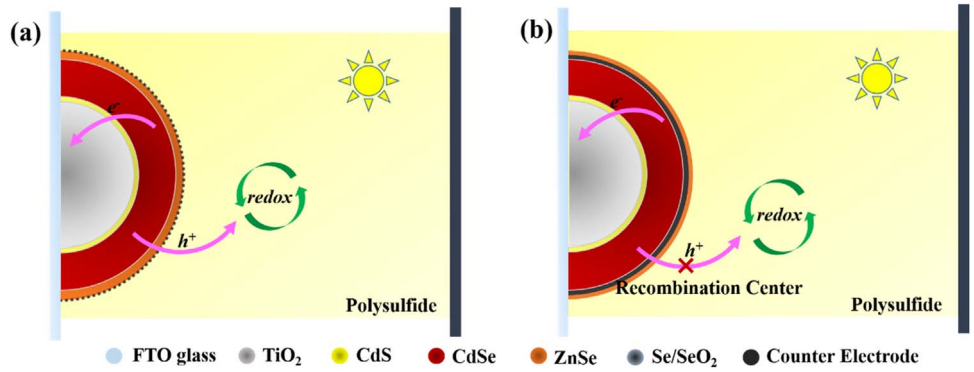

Scheme 2. Schematic illustration of the photo induced charge-transfer processes of the TiO_2/CdS/CdSe QDSCs deposited with three cycles of SILAR in (a) Zn^{2+} initiated sequence and (b) Se^{2-} -initiated sequence.

and inside QDs, which would severely hinder the performance of the device.

As reported in literatures,[3,60] the performance of the solar cells was mainly determined by the capability of light absorption and charge transfer and collection. The light absorption spectra is shown in Fig. 4; there is almost no difference for the samples with various cycles of SILAR in different immersion sequences. So the strong dependence of the cell performance on the SILAR deposition sequence is most likely due to the capability of charge transfer and charge collection, as supported by the EIS results. In the QDSCs with Zn^{2+}-initiated ZnSe deposition, the ZnSe/Se/SeO_2 layer acts as a barrier layer to hinder the charge recombination, as reflected by the appreciable increase of charge recombination resistance as determined via EIS measurement. To the contrary, for the QDSCs with Se^{2-}-initiated ZnSe deposition, Se/SeO_2/ZnSe layer introduces a negative effect on the photovoltaic properties. SeO_2/Se layer between QDs and ZnSe acts as a recombination site with reduced charge recombination resistance.

In the present study, aqueous solvent is used and the photoanodes have to be rinsed with water and dried after dipping in the precursor solution, it is difficult to conduct all these synthesis in totally inert oxygen free environment such as in a glove box. Synthesis of quantum dots or fabrication of buffer or surface layers inside the glovebox will mark a significant departure from our current experimental condition such as the solvent evaporation rate would be much higher, so the results would be very different for the comparison purpose. However, we are going to run the follow up experiments in inert environment and possibly publish the results in the future to further clarify and verify the results reported in this paper.

3. Conclusions

In the ZnSe passivation layer deposition process, different SILAR immersion cycles and sequences would have vital influence on the photovoltaic properties of the corresponding solar cells. During the SILAR immersion, Se^{2-} was unintentionally oxidized to Se^0 or SeO_2. With SILAR in Zn^{2+}-initiated sequence, in spite of a small amount of Se^0 and SeO_2 formed during the SILAR process, the photovoltaic performance was much improved due to enhanced light absorption and reduced charge recombination. With SILAR in Se^{2-}-initiated sequence, only a small amount of ZnSe was formed, and most of the Se^{2-} were oxidized into Se^0 and SeO_2. Although the light absorption was enhanced, excessive Se^0 and SeO_2 would act as a recombination site and serve as a barrier hindering charge transfer. The present study gives a better understanding on how the difference in the chemical composition and interfacial structure of ZnSe passivation layer could influence the performance of QDSCs.

4. Experimental methods

4.1. Chemicals and materials

Titanium oxide (TiO_2, Degussa, P25), α–terpineol ($C_{10}H_8O$, 96%, Sigma Aldrich), ethyl cellulose ($[C_6H_7O_2(OC_2H_5)_3]n$, 48.0–49.5% (w/w) as ethoxyl, Sigma Aldrich), Zinc acetate dihydrate ($Zn(AC)_2{\cdot}2H_2O$, AR, 98.0%), cadmium acetate dihydrate ($Cd(AC)_2{\cdot}2H_2O$, AR, 98.0%), cadmium nitrate tetrahydrate ($Cd(NO_3)_2{\cdot}4H_2O$, AR, 98.0%), sodium sulfide (Na_2S, AR, 98.0%), sodium borohydride ($NaBH_4$, AR, 98.0%), selenium powder (Se, −200 mesh, 3 N, 99.9%), and sulfur (S, Reagent grade). brass foil (alloy 260, 0.3 mm thick, Alfa Aesar), hydrochloric acid (HCl, 37%, USA), methanol (CH_3OH, ≥99.5%, Sigma Aldrich), and ethanol (CH_3COOH, ≥99.5%, Decon) were all used as received. Ultrapure deionized water was used for the preparation of all aqueous solutions.

4.2. Preparation of the TiO_2/CdS/CdSe photoanode with a ZnSe passivation layer

The preparation of mesoporous TiO_2 films and the growth of CdS/CdSe QDs were all according to the previous publication [44,52,61]. In brief, the mesoporous TiO_2 film was made by doctor blading a TiO_2 paste on the F: SnO_2-coated (FTO, 6-8 Ω/square) glass substrate followed with sintering at 500 °C for 30 min. The CdS QDs were deposited by successive ionic layer adsorption and reaction (SILAR) method with five cycles on the surface of TiO_2 mesoporous films. The CdSe QDs were deposited on the TiO2/CdS film through a chemical bath deposition (CBD) procedure under dark condition for 3 h at room temperature.

The ZnSe layers with different deposition sequences were also deposited by SILAR method. More specifically, for Zn^{2+} initiated sequence, the substrate QD sensitized photoanodes were first immersed in 0.1 M Zn^{2+} precursor solution for 2 min, rinsing with DI water and drying, and subsequently the films were immersed in 0.1 M Se^{2-} solution for 2 min, rinsing with DI water and drying again to complete the deposition of one ZnSe layer, and this entire process was defined as one SILAR cycle. For Se^{2-}-initiated sequence, the substrate QD sensitized photoanodes were first immersed in 0.1 M Se^{2-} precursor solution, then in Zn^{2+} precursor solution. In this process Se source solution was always purged with N_2.

4.3. Electrolyte, counter electrode and device assembly

The polysulfide electrolyte were prepared by dissolving 1 M sulfur and 1 M sodium sulfide in 10 mL deionized water. The Cu_2S counter electrode was made by immersing a brass foil into hydrochloric acid at 80 °C for 40 min to remove Zinc and then immersing it into the freshly prepared electrolyte for 5 min to form Cu_2S. The device was assembled

into sandwich-type using a scotch tape placed between the QDs sensitized photoanode and counter electrode.

4.4. Characterization

The morphology of the films was characterized by scanning electron microscope (SEM, JSM-7000). The compositional EDX analysis and elemental mapping on the samples were carried out by EDX integrated in SEM (JSM-7000). The photovoltaic properties were measured using an HP 4155A programmable semiconductor parameter analyzer under AM 1.5 simulated sunlight with a power density of 100 mW cm^{-2}. The X-ray photoelectron spectra (XPS) were collected using a Thermo ESCALAB 250XI spectrometer. The Optical absorption (Perkin Elmer Lambda 900 UV/VIS/IR Spectrometer) was used to study the light absorption properties of the samples. Electrochemical impedance spectroscopy (EIS) was carried out using a Solartron 1287 A coupled with a Solartron 1260 FRA/impedance analyzer to investigate the electronic and ionic processes in the QDSCs.

Acknowledgments

This work was financially supported by the National Science Foundation (NSF, DMR 1505902) and Fei Huang and Hongen Wang would also like to acknowledge the scholarship by China Scholarship Council for the scholarship. This work was also supported by National Natural Science Foundations of China (Nos. 21377023, 51362026 and 21477019).

References

[1] Q. Zhang, G. Cao, Nano Today 6 (2011) 91–109.
[2] G. Niu, W. Li, J. Li, L. Wang, Sci. Chin. Mater. 59 (2016) 728–742.
[3] J.J. Tian, G.Z. Cao, Coord. Chem. Rev. 320 (2016) 193–215.
[4] B. Oregan, M. Gratzel, Nature 353 (1991) 737–740.
[5] T.P. Chou, Q. Zhang, G.E. Fryxell, G.Z. Cao, Adv. Mater. 19 (2007) 2588–2592.
[6] Q. Zhang, T.P. Chou, B. Russo, S.A. Jenekhe, G. Cao, Angew. Chem. Int. Ed. 47 (2008) 2402–2406.
[7] P.V. Kamat, J. Phys. Chem. C 112 (2008) 18737–18753.
[8] Y.-L. Lee, Y.-S. Lo, Adv. Funct. Mater. 19 (2009) 604–609.
[9] H. Lee, M.K. Wang, P. Chen, D.R. Gamelin, S.M. Zakeeruddin, M. Gratzel, M.K. Nazeeruddin, Nano Lett. 9 (2009) 4221–4227.
[10] S. Ruhle, M. Shalom, A. Zaban, Chemphyschem 11 (2010) 2290–2304.
[11] W. Shockley, H.J. Queisser, J. Appl. Phys. 32 (1961) 510–519.
[12] Z.F. Yu, S. Sandhu, S.H. Fan, Nano Lett. 14 (2014) 66–70.
[13] M.C. Hanna, A.J. Nozik, J. Appl. Phys. 100 (2006) 074510.
[14] S. Mathew, A. Yella, P. Gao, R. Humphry-Baker, B.F.E. Curchod, N. Ashari-Astani, I. Tavernelli, U. Rothlisberger, M.K. Nazeeruddin, M. Graetzel, Nat. Chem. 6 (2014) 242–247.
[15] Z.L. Du, Z.X. Pan, F. Fabregat-Santiago, K. Zhao, D.H. Long, H. Zhang, Y.X. Zhao, X.H. Zhong, J.S. Yu, J. Bisquert, J. Phys. Chem. Lett. 7 (2016) 3103–3111.
[16] H.A. Atwater, A. Polman, Nat. Mater. 9 (2010) 205–213.
[17] J. Wu, P. Yu, A.S. Susha, K.A. Sablon, H. Chen, Z. Zhou, H. Li, H. Ji, X. Niu, A.O. Govorov, A.L. Rogach, Z.M. Wang, Nano Energy 13 (2015) 827–835.
[18] T. Kawawaki, H. Wang, T. Kubo, K. Saito, J. Nakazaki, H. Segawa, T. Tatsuma, ACS Nano 9 (2015) 4165–4172.
[19] Q. Zhang, J. Nanophotonics 4 (2010) 041540.
[20] J. Tian, L. Lv, X. Wang, C. Fei, X. Liu, Z. Zhao, Y. Wang, G. Cao, J. Phys. Chem. C 118 (2014) 16611–16617.
[21] J. Tian, G. Cao, J. Phys. Chem. Lett. 6 (2015) 1859–1869.
[22] X. Lan, O. Voznyy, A. Kiani, F.P.G. de Arquer, A.S. Abbas, G.-H. Kim, M. Liu, Z. Yang, G. Walters, J. Xu, M. Yuan, Z. Ning, F. Fan, P. Kanjanaboos, I. Kramer, D. Zhitomirsky, P. Lee, A. Perelgut, S. Hoogland, E.H. Sargent, Adv. Mater. 28 (2016) 299–304.
[23] K. Zhao, Z. Pan, X. Zhong, J. Phys. Chem. Lett. 7 (2016) 406–417.
[24] Y. Cao, A. Stavrinadis, T. Lasanta, D. So, G. Konstantatos, Nat. Energy 1 (2016) 16035.
[25] Z. Ren, J. Wang, Z. Pan, K. Zhao, H. Zhang, Y. Li, Y. Zhao, I. Mora-Sero, J. Bisquert, X. Zhong, Chem. Mater. 27 (2015) 8398–8405.
[26] J. Tian, Q. Zhang, E. Uchaker, R. Gao, X. Qu, S. Zhang, G. Cao, Energy Environ. Sci. 6 (2013) 3542.
[27] K. Zhao, Z. Pan, I. Mora-Sero, E. Canovas, H. Wang, Y. Song, X. Gong, J. Wang, M. Bonn, J. Bisquert, X. Zhong, J. Am. Chem. Soc. 137 (2015) 5602–5609.
[28] L. Li, X.C. Yang, J.J. Gao, H.N. Tian, J.Z. Zhao, A. Hagfeldt, L.C. Sun, J. Am. Chem. Soc. 133 (2011) 8458–8460.
[29] N. Fuke, L.B. Hoch, A.Y. Koposov, V.W. Manner, D.J. Werder, A. Fukui, N. Koide, H. Katayama, M. Sykora, ACS Nano 4 (2010) 6377–6386.
[30] L.-B. Li, W.-Q. Wu, H.-S. Rao, H.-Y. Chen, H.-L. Feng, D.-B. Kuang, C.-Y. Su, Sci. Chin. Mater. 59 (2016) 807–816.
[31] H. Li, S. Jiao, J. Ren, H. Li, S. Gao, J. Wang, D. Wang, Q. Yu, Y. Zhang, L. Li, Phys. Chem. Chem. Phys. 18 (2016) 4144–4153.
[32] S. Kim, A.R. Marshal, D.M. Kroupa, E.M. Miller, J.M. Luther, S. Jeong, M.C. Beard, ACS Nano 9 (2015) 8157–8164.
[33] W. Li, J. Yang, M. Liu, Y. Luo, Y. Xiao, L. Fu, S. Wu, J. Electrochem. Soc. 161 (2014) D510–D514.
[34] X. Xu, Q. Wan, C. Luan, F. Mei, Q. Zhao, P. An, Z. Liang, G. Xu, J.A. Zapien, ACS Appl. Mater. Interfaces 5 (2013) 10605–10613.
[35] I. Robel, V. Subramanian, M. Kuno, P.V. Kamat, J. Am. Chem. Soc. 128 (2006) 2385–2393.
[36] K. Yan, W. Chen, S. Yang, J. Phys. Chem. C 117 (2013) 92–99.
[37] R. Zhou, H. Niu, Q. Zhang, E. Uchaker, Z. Guo, L. Wan, S. Miao, J. Xu, G. Cao, J. Mater. Chem. A 3 (2015) 12539–12549.
[38] R. Zhou, Q. Zhang, J. Tian, D. Myers, M. Yin, G. Cao, J. Phys. Chem. C 117 (2013) 26948–26956.
[39] J. Du, Z. Du, J.S. Hu, Z. Pan, Q. Shen, J. Sun, D. Long, H. Dong, L. Sun, X. Zhong, L.J. Wan, J. Am. Chem. Soc. (2016). http://dx.doi.org/10.1021/jacs.6b00615.
[40] W. Li, X. Zhong, J. Phys. Chem. Lett. 6 (2015) 796–806.
[41] H. Zhang, K. Cheng, Y.M. Hou, Z. Fang, Z.X. Pan, W.J. Wu, J.L. Hua, X.H. Zhong, Chem. Commun. 48 (2012) 11235–11237.
[42] M.A. Becker, J.G. Radich, B.A. Bunker, P.V. Kamat, J. Phys. Chem. Lett. 5 (2014) 1575–1582.
[43] H.-S. Rao, W.-Q. Wu, Y. Liu, Y.-F. Xu, B.-X. Chen, H.-Y. Chen, D.-B. Kuang, C.-Y. Su, Nano Energy 8 (2014) 1–8.
[44] F. Huang, J. Hou, Q. Zhang, Y. Wang, R.C. Massé, S. Peng, H. Wang, J. Liu, G. Cao, Nano Energy 26 (2016) 114–122.
[45] F. Huang, Q. Zhang, B. Xu, J. Hou, Y. Wang, R.C. Massé, S. Peng, J. Liu, G. Cao, J. Mater. Chem. A 4 (2016) 14773–14780.
[46] B. Canava, J. Vigneron, A. Etcheberry, J.F. Guillemoles, D. Lincot, Appl. Surf. Sci. 202 (2002) 8–14.
[47] S. Lopez-Marino, Y. Sanchez, M. Placidi, A. Fairbrother, M. Espindola-Rodriguez, X. Fontane, V. Izquierdo-Roca, J. Lopez-Garcia, L. Calvo-Barrio, A. Perez-Rodriguez, E. Saucedo, Chem.-Eur. J. 19 (2013) 14814–14822.
[48] B.O. Dabbousi, J. RodriguezViejo, F.V. Mikulec, J.R. Heine, H. Mattoussi, R. Ober, K.F. Jensen, M.G. Bawendi, J. Phys. Chem. B 101 (1997) 9463–9475.
[49] J. Xu, C.Y. Luan, Y.B. Tang, X. Chen, J.A. Zapien, W.J. Zhang, H.L. Kwong, X.M. Meng, S.T. Lee, C.S. Lee, ACS Nano 4 (2010) 6064–6070.
[50] B. Wang, T. Liu, C. Xia, F. Zhou, F. He, R. Liu, Y. Hu, H. Wang, Mater. Res. Bull. 59 (2014) 234–240.
[51] J. Tian, Q. Zhang, L. Zhang, R. Gao, L. Shen, S. Zhang, X. Qu, G. Cao, Nanoscale 5 (2013) 936–943.
[52] J. Tian, R. Gao, Q. Zhang, S. Zhang, Y. Li, J. Lan, X. Qu, G. Cao, J. Phys. Chem. C 116 (2012) 18655–18662.
[53] S. Verma, S. Kaniyankandy, H.N. Ghosh, J. Phys. Chem. C 117 (2013) 10901–10908.
[54] B.C. Fitzmorris, J.K. Cooper, J. Edberg, S. Gul, J. Guo, J.Z. Zhang, J. Phys. Chem. C 116 (2012) 25065–25073.
[55] K. Wang, J. Chen, W. Zhou, Y. Zhang, Y. Yan, J. Pern, A. Mascarenhas, Adv. Mater. 20 (2008) 3248–3253.
[56] R. Ahmed, L. Zhao, A.J. Mozer, G. Will, J. Bell, H. Wang, J. Phys. Chem. C 119 (2015) 2297–2307.
[57] M. Zhu, F. Hao, L. Ma, T.-B. Song, C.E. Miller, M.R. Wasielewski, X. Li, M.G. Kanatzidis, ACS Energy Lett. 1 (2016) 469–473.
[58] J. van de Lagemaat, N.G. Park, A.J. Frank, J. Phys. Chem. B 104 (2000) 2044–2052.
[59] R. Kern, R. Sastrawan, J. Ferber, R. Stangl, J. Luther, Electrochim. Acta 47 (2002) 4213–4225.
[60] H. Zhao, F. Huang, J. Hou, Z. Liu, Q. Wu, H. Cao, Q. Jing, S. Peng, G. Cao, ACS Appl. Mater. Interfaces 8 (2016) 26675–26682.
[61] Z. Yang, Q. Zhang, J. Xi, K. Park, X. Xu, Z. Liang, G. Cao, Sci. Adv. Mater. 4 (2012) 1013–1017.

Fei Huang is a Ph.D. candidate under the supervision of Prof. Jianshe Liu at Donghua University, China. She is currently a visiting student under the supervision of Prof. Guozhong Cao at University of Washington, Seattle. Her recent research mainly focuses on the synthesis and surface modification of the photoanode materials in quantum dot sensitized solar cells.

Juan Hou earned her Ph.D. degree from University of Chinese Academy of Sciences in 2003. Currently she is an assistant professor in College of Science at Shihezi University, China. Her current research focuses on quantum dots and their application in photovoltaic conversion devices.

Hongen Wang received his Bachelor degree from Taiyuan University of Technology in 2003, MPhil degree from Central South University in 2007, and Ph.D. degree from City University of Hong Kong in 2012. He is now as associate professor at State Key Laboratory of Advanced Technology for Materials Synthesis and Processing, Wuhan University of Technology, Wuhan, Hubei, China. He is currently also a visiting scholar at Department of Materials Science and Engineering, University of Washington, Seattle, WA, US. His current research interests mainly focus on anode materials for Li/Na ion batteries, Li-S batteries, inorganic solid electrolyte materials for all solid-state lithium batteries, and nanostructured photoanodes for quantum-dot sensitized solar cells.

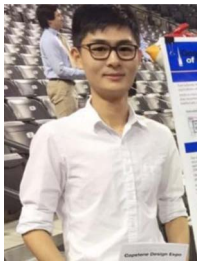

Hao Tang earned his master's degree from University of Washington in 2016 and his bachelor's degree from Georgia Institute of Technology in 2015. He is currently working in Prof. Guozhong Cao's group. His research interests are in the field of photovoltaic devices, including quantum dot sensitized solar cells, colloidal quantum dot solar cells and perovskite solar cells.

Zhaoyu Liu is an undergraduate student in chemistry major of University of Washington, Seattle. She is currently a research student under the supervision of Prof. Guozhong Cao in Department of Material Science and Engineering. Her research focuses on quantum dot sensitized solar cells.

Lisha Zhang received her B.S. degree (2002) and M.S. degree (2005) in Chemistry from Central China Normal University, China. Then, she worked as research assistant in Shanghai Institute of Ceramics, Chinese Academy of Sciences for two years. In 2007, she started Ph.D. study in Chinese University of Hong Kong and received her Ph.D. degree in 2010. Subsequently, she joined College of Environmental Science and Engineering, Donghua University in Shanghai. Her research interests include the synthesis of nanomaterials, construction of photovoltaic devices, photocatalytic technology and its applications in environmental protection, and environmental biotechnology.

Qifeng Zhang is currently working at University of Washington as a Research Assistant Professor. His research interests involve engineering applications of nanostructured materials on electrical devices including solar cells, UV light-emitting diodes (LEDs), eld-effect transistors (FETs), and gas sensors. His current research focuses on the synthesis of nanomaterials and the application of nanomaterials in electronic and optoelectronic devices, such as dye-sensitized solar cells (DSCs) and organic/inorganic hybrid solar cells.

Shanglong Peng is an associate professor of School of Physical Science and Technology at Lanzhou University. His current research is focused mainly on new energy materials and devices including Si-based inorganic-organic hybrid solar cells, quantum dot sensitized solar cells and supercapacitor. And he has published over 50 papers.

Dr. Jianshe Liu is Dean of the College of Environmental Science and Engineering, and Professor of Environmental Science, at Donghua University. He has published more than 100 peer-reviewed articles. His recent research mainly focuses on environmental biotechnology, advanced oxidation technology, functional nanostructured materials and their applications in photocatalysis and solar cells.

Guozhong Cao is Boeing-Steiner Professor of materials science and engineering, professor of chemical engineering, and adjunct professor of mechanical engineering at the University of Washington, and also a professor at Beijing Institute of Nanoenergy and Nanosystems, Chinese Academy of Sciences and Dalian University of Technology. His current research is focused on chemical processing of nanomaterials for energy related applications including solar cells, rechargeable batteries, supercapacitors, and hydrogen storage.